International Journal of Mass Spectrometry 302 (2011) 116–124

Contents lists available at ScienceDirect

International Journal of Mass Spectrometry

journal homepage: www.elsevier.com/locate/ijms

Complexation and calcium-induced conformational changes in the cardiac troponin complex monitored by hydrogen/deuterium exchange and FT-ICR mass spectrometry

George M. Bou-Assaf[a], Jean E. Chamoun[b], Mark R. Emmett[a,1], Piotr G. Fajer[b], Alan G. Marshall[a,*,1]

[a] Department of Chemistry and Biochemistry, Florida State University, Tallahassee, FL 32306, United States
[b] Institute of Molecular Biophysics, Florida State University, Tallahassee, FL 32306, United States

ARTICLE INFO

Article history:
Received 5 June 2010
Received in revised form 18 August 2010
Accepted 30 August 2010
Available online 9 September 2010

Keywords:
Isotopic depletion
H/D exchange
FTMS
Fourier transform
Ion cyclotron resonance

ABSTRACT

Cardiac muscle contraction is regulated by the heterotrimeric complex: troponin. We apply solution-phase hydrogen/deuterium exchange monitored by FT-ICR mass spectrometry to study the structural dynamics and the Ca-induced conformational changes of the cardiac isoform of troponin, by comparing H/D exchange rate constants for TnC alone, the binary TnC:TnI complex, and the ternary TnC:TnI:TnT complex for Ca-free and Ca-saturated states. The wide range of exchange rate constants indicates that the complexes possess both highly flexible and very rigid domains. Fast exchange rates were observed for the N-terminal extension of TnI (specific to the cardiac isoform), the DE linker in TnC alone, and the mobile domain of TnI. The slowest rates were for the IT coiled-coil that grants stability and stiffness to the complex. Ca^{2+} binding to site II of the N-lobe of TnC induces short-range allosteric effects, mainly protection for the C-lobe of TnC that transmits long-range conformational changes that reach the IT coiled-coil and even TnT1. The present results corroborate prior X-ray crystallography and NMR interpretations and also illuminate domains that were truncated or not resolved in those experiments.

Published by Elsevier B.V.

1. Introduction

Muscles are composed of fibers that consist of long myofibrils. The smallest functional unit of a muscle, the sarcomere, is composed of thin and thick filaments. Actin, tropomyosin (Tm), and the troponin complex (Tn) are the main components of the thin filament, whereas myosin is the major protein found in the thick filament. Tn is a 77 kDa heterotrimeric complex with a calcium-binding subunit, troponin C (TnC); an inhibitory subunit, troponin I (TnI), and troponin T (TnT) which plays a role in anchoring the complex to the rest of the thin filament (reviewed in [1]).

TnC is a Ca^{2+} sensor protein that belongs to the EF hand (helix-loop-helix motif) family. It has a dumbbell shape with N- and C-terminal lobes connected by a flexible central helix (Fig. 1a). The structural domain (C-lobe) has two high affinity Ca^{2+}/Mg^{2+} binding sites (III and IV) that preferentially bind Mg^{2+} at sub-micromolar Ca^{2+} concentration ($<10^{-5}$ M). The regulatory domain (N-lobe) has low metal affinity with high Ca^{2+} selectivity. The binding of Ca^{2+} to the N-lobe induces the opening of a hydrophobic cleft due to the reorientation of helices B and C relative to the N, A and D helices [1–5]. Those conformational changes are translated to the rest of Tn and eventually lead to muscle contraction. The dissociation of Ca^{2+} has the opposite effect on helices B and C and promotes muscle relaxation. TnC exists in two different isoforms, skeletal (sTnC) and cardiac (cTnC). Both have the same dumbbell shape, but the cardiac isoform has only one active Ca^{2+} binding site (site II) in the regulatory domain vs. two (sites I and II) for the skeletal counterpart. The linker between the N- and the C-lobes is disordered in cTnC [5] but adopts a rigid helical structure in sTnC [6]. In addition, Ca-induced movement in the N-lobe (see above) is more pronounced in sTnC [7–9].

TnI is responsible for inhibition of the acto-myosin ATPase activity: hence its name, "inhibitory subunit". Two isoforms of TnI differ mainly by the presence of an N-terminal extension in cardiac TnI, ranging from 30 to 33 amino acids depending on the species. Two Protein Kinase A (PKA) phosphorylation sites (serine 22 and 23) in that extension are believed to decrease Tn Ca sensitivity [10,11]. Two long helices 1 and 2 in TnI (Fig. 1b) participate in binding to TnC and TnT. The inhibition effect of TnI is thought to result mainly from the binding of an inhibitory peptide (aa 138–147) to the N-terminal region of actin [12]. An amphiphilic "switch peptide" (aa 150–160) lies upstream from the inhibitory peptide with the ability to bind to the hydrophobic pocket of TnC in the Ca-saturated state [13,14]. In

* Corresponding author. Tel.: +1 850 644 0529; fax: +1 850 644 1366.
E-mail address: marshall@magnet.fsu.edu (A.G. Marshall).
[1] Also a member of the Ion Cyclotron Resonance Program, National High Magnetic Field Laboratory, Florida State University, 1800 East Paul Dirac Dr., Tallahassee, FL 32310-4005, United States.

1387-3806/$ – see front matter. Published by Elsevier B.V.
doi:10.1016/j.ijms.2010.08.023

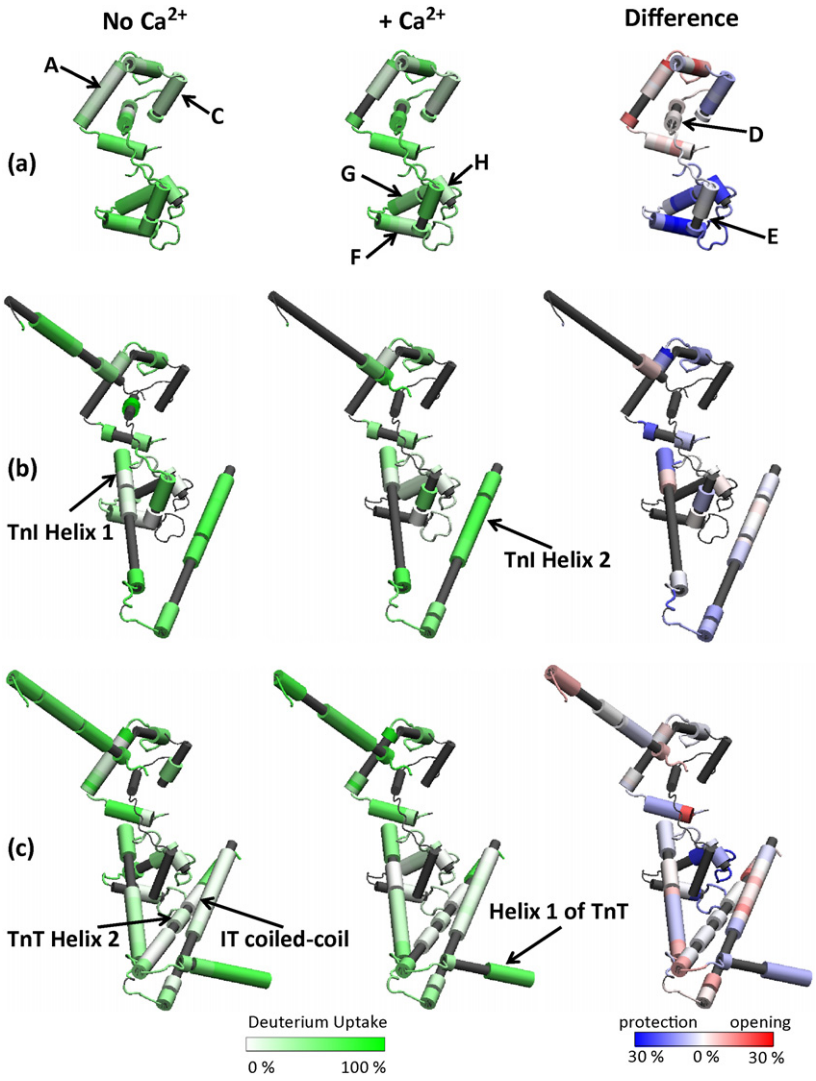

Fig. 1. Deuterium uptake mapped on the Ca-saturated crystal structure of Takeda et al. [5] after 30 s of exchange in D_2O: (a) TnC alone, (b) binary complex (TnC:TnI) and (c) ternary complex (TnC:TnI:TnT). HDX was performed in the Ca-free state (left), and the Ca-saturated state (middle). Gray segments of the crystal structure represent areas not covered by the proteolytic digestion. Elsewhere, the greener the color, the higher the deuterium uptake. The difference in deuterium uptake (right) represents the Ca-induced conformational changes: protection in blue and exposure in red.

the Ca-free state, the position and structure of the switch peptide is not known. Another possible site of interaction with actin lies at the C-terminal end of TnI, also known as the mobile domain. That segment is known to be highly flexible based on a recent NMR study [15] of the skeletal isoform and is not resolved in the Tn crystal structure [5].

TnT plays a major role in connecting all of the subunits of the Tn complex. TnT is ~17 nm long and consists of an acidic N-terminal (TnT1) and a basic C-terminal region (TnT2). TnT1 binds strongly to Tm and is responsible for the cooperative transition of the thin filament. TnT2 possesses two helices, 1 and 2 and binds TnI, TnC and Tm [16,17]. Helix 2 of TnT2 and helix 2 of TnI wrap around each other to form the so-called IT coiled-coil. TnT and TnI helices form a W shape wrapped around the C-lobe of TnC (Fig. 1c).

Numerous structural studies have focused on the conformational changes in the TnC subunit [18–21], the binary complex [9,22,23], and more recently the ternary complex [5,6] upon Ca^{2+} binding and dissociation. Unfortunately, many important regions of the Tn complex were either not included or not resolved. Here, we apply solution-phase hydrogen/deuterium exchange (HDX) monitored by mass spectrometry to characterize the complexation of Tn and the effect of Ca^{2+} binding on the entire complex. HDX is a fast and sensitive method to study protein dynamics and higher-order structural changes upon ligand binding [24–26]. Briefly, the technique consists in incubating the protein or complex in deuterated water for each of several time periods, after which the exchange is quenched by lowering the pH, and the protein digested by a protease. The rate constant(s) for H/D exchange are determined from the mass increase as a function of H/D exchange period for each proteolytic fragment. Fourier transform ion cyclotron resonance (FT-ICR) [27,28] is the mass analyzer of choice because it provides ultrahigh mass resolving power and sub-ppm mass accuracy ($m/\Delta m_{50\%}$ = 200,000 at m/z 400, in which m is the ion mass and $\Delta m_{50\%}$ is the mass spectral peak full width at half-maximum peak height) needed to confidently assign each experimental mass to the corresponding proteolytic fragment. Although HDX monitored by FT-ICR was recently used in an independent work to study the Tn complex, [29] HDX was performed on the ternary complex that lacked TnT1, and little was known about the TnI N-terminal extension which was observed only in the Ca-saturated state.

Here, we characterize the interactions between the subunits of Tn and the consequent segment-specific changes in solvent accessibility based on HDX for TnC alone, the binary complex (TnC:TnI), and the ternary complex (TnC:TnI:TnT). In addition, we monitor the

allosteric effects induced by Ca^{2+} binding to the N-lobe of TnC. We find that the Tn complex comprises highly flexible domains (TnI N-terminal extension and mobile domain) and very stable structures (IT coiled-coil). Moreover, Ca^{2+} induces short-range protection in the C-lobe of TnC and long-range effects that extend to the IT coiled-coil.

2. Materials and methods

2.1. Materials

Deuterium oxide D_2O (99.9%), formic acid, and protease type XIII from *Aspergillus satoi* were obtained from Sigma–Aldrich (St. Louis, MO, USA). Tris, MOPS, NaCl, KCl, $MgCl_2$, $MgSO_4$, urea, and ultrahigh-purity HPLC solvents (water and acetonitrile) for mass spectrometric analysis were obtained from VWR International (Suwanee, GA, USA).

2.2. Protein expression and purification

Plasmid vectors, which carry the genes of the Tn complex subunits, were expressed and purified separately from *Escherichia coli* bacteria (BL21 DE3 strain) as described previously [30–32]. Proteins with natural abundance isotopes were expressed in Luria Broth (LB) medium. In addition, TnC and TnI were isotopically depleted in ^{13}C for fragment identification (see [33]). Depleted proteins were obtained by expression in minimal medium (M9) in which the only source of carbon is ^{13}C-depleted glucose. The M9 medium was prepared in 10 mM phosphate buffer at pH 7.5, 10 mM NaCl, 20 mM $(NH_4)_2SO_4$, 2 mM $MgSO_4$, 0.1 mM $CaCl_2$, 5 μM $FeCl_3$, 4 g/L glucose and 3 mM vitamin B1. The BL21 cells were grown in the presence of ampicillin at 37 °C. At an optical density (OD) of ~0.6 at 600 nm, the expression was induced with isopropyl β-D-1-thiogalactopyranoside and allowed to proceed for an additional 4 h. The medium was centrifuged and the pellet was resuspended in the appropriate lysis buffer for purification according to protocols previously described [30–32].

2.3. Sample preparation: complex reconstitution

To map the sites of interaction between subunits of the Tn binary and ternary complexes as well as to study the effect of Ca^{2+} binding to the TnC subunit, we performed HDX experiments on TnC, TnC:TnI, and TnC:TnI:TnT. Equimolar amounts of TnC and TnI, or TnC, TnI, and TnT were mixed to form the binary and the ternary complexes respectively. Consecutive dialysis steps eliminated the original denaturing agent. The final reconstitution buffer was: 50 mM MOPS in the presence of 0.1 M KCl and 3 mM $MgCl_2$ at pH 7.2. For the Ca-free state, 1 mM EGTA was added to 50 μM of each sample to eliminate any residual Ca^{2+}. For the Ca-saturated state, 1 mM $CaCl_2$ was added to 50 μM of each sample. ($K_d = 2 \times 10^{-5}$ M^{-1} for binding of Ca^{2+} to TnC alone, and 5×10^{-6} M^{-1} for TnC:TnI and TnC:TnI:TnT [34].)

2.4. Hydrogen/deuterium exchange and mass spectrometric analysis

Each of the above-mentioned complexes was diluted 10-fold in either H_2O buffer for the control or the D_2O buffer for the exchange data points. Exchange was allowed to proceed for 30 s, 1 min, 2 min, 4 min, 8 min, 15 min, 30 min, 1 h, 2 h, 4 h and 8 h at ~0 °C to reduce the rate of the fastest exchanging amide hydrogens. The exchange was quenched and the complex digested for 2 min by adding protease XIII (1:1 (v/v)) in 2% formic acid at a concentration of 4.5 mg/mL. The final pH meter reading for the solution was ~2.3. For more efficient digestion of the ternary complex, 4 M urea was added to the quench solution [35]. The digest was injected onto a ProZap C_{18} column and eluted at 300 μL/min with a short, 1.5 min gradient (2–95% acetonitrile) to minimize back-exchange [36]. The eluent was post-column split (1:100) and introduced into a hybrid 14.5 T LTQ-FT-ICR mass spectrometer by micro-electrospray ionization [37]. Data were collected by X-calibur software (Thermo-Fisher). All steps of the HDX experiment were automated by a robot (LEAP technologies) to eliminate human error and standardize timing. Every experiment was run in triplicate to determine reproducibility [38].

2.5. Fragment identification and data analysis

Data were analyzed by a custom analysis procedure [39] in which the deuterium uptake for each exchange period for each proteolytic fragment was calculated by taking the difference between the average mass of the deuterated fragment at a given exchange period and the average mass of the control (undeuterated fragment). Deuterium uptake was scaled relative to the maximum number of exchanging hydrogens and data are reported in percent deuterium uptake.

Isotopic depletion aids significantly in fragment identification [33]. Briefly, proteolytic digestion produces dozens of fragments, some of which are isomeric/isobaric. In other words, the same m/z value could be assigned to a segment from more than one subunit of the Tn binary or ternary complex. With isotopic depletion, the near disappearance (or not) of species containing ^{13}C in the isotopic distribution establishes that the peptide in question does (or does not) belong to the depleted subunit protein (see [33]).

Each deuterium uptake vs. time profile was fitted to a single exponential or sum of two exponentials to yield average rate constants for each proteolytic fragment (see Supplemental Tables). For a given peptide, an improvement of 15% or more in X^2 for the double exponential relative to single-exponential fit implies that two populations of amide hydrogens are exchanging with significantly different rate constants. (A three-exponential fit did not significantly improve X^2 for any peptide.) Overlapping fragments that exhibited similar rate constants were grouped together and the average rate constant is reported.

3. Results

Hydrogen/deuterium exchange was performed for TnC alone, the binary TnC:TnI complex and the ternary TnC:TnI:TnT complex in the presence and absence of Ca^{2+}. Fig. 1 shows deuterium uptake after 30 s of H/D exchange, mapped on the Tn complex Ca-saturated crystal structure of Takeda et al. [5]. The deuterium uptake for the Ca-free state (left) was subtracted from that in the Ca-saturated state (middle) to show the difference between both states (right) and thus emphasize the Ca-induced conformational changes. Deuterium uptake is normalized to the maximum number of exchangeable amide hydrogens per proteolytic fragment and is represented in green from 0% to 100% on the left and middle panels. Thinner gray segments represent protein segments not accessed by proteolysis. In the right panel, lower deuterium incorporation on addition of Ca^{2+} represents Ca-induced protection (blue) and higher incorporation represents Ca-induced exposure (red).

Rate constants were computed from the deuterium uptake data for each H/D exchange period (see Section 2). Tables 1–3 report the exchange rate constants (in h^{-1}) for TnC alone, the binary TnC:TnI complex and the ternary TnC:TnI:TnT complex, in the presence and the absence of Ca^{2+}. For double-exponential fits, the percentage of observed exchangeable hydrogens corresponding to each rate constant is reported. The exponential-fit statistical figures of merit for

Table 1
Hydrogen/deuterium exchange rate constants for TnC alone in the Ca-free and Ca-saturated states. Some fragments exchange with two different rate constants, others with only one. The percentage in parentheses represents the population of amide hydrogens that resulted from a double-exponential fit.

TnC	Rate for Ca-free (h^{-1})	TnC	Rate for Ca-saturated (h^{-1})
1–8	3000	1–15	1900
9–14	310		
15–27	1.7 (35%) and 0.15 (65%)	16–27	0.35
28–41	1500 (80%) and 5.4 (20%)	28–43	3500 (90%) and 1.62 (10%)
42–74	190 (55%) and 0.72 (45%)	47–52	1300
53–57	140 (50%) and 0.53 (50%)		
		61–74	1200 (80%) and 5.9 (20%)
81–100	1700	82–100	1900
101–113	1200	105–114	1300 (45%) and 0.47 (55%)
114–120	2100 (75%) and 35 (25%)	117–120	0.40
121–148	3000	121–132	2500
		133–149	5100 (80%) and 0.29 (20%)
150–161	360	150–153	5900 (5%) and 0.032 (95%)
		154–161	180 (70%) and 3.3 (30%)

each proteolytic fragment in each subunit (TnC, TnI or TnT) and state (TnC alone, TnC:TnI, TnC:TnI:TnT in the presence and the absence of Ca^{2+}) are listed in the Supplemental Tables in the online version of this manuscript.

3.1. TnC alone

The proteolytic digestion of TnC alone produced 140 peptides with an average length of ~10 aa/fragment, and sequence coverage was greater than 95% for both the Ca-free and the Ca-saturated states. After 8 h of incubation in heavy water, all segments of TnC exchanged almost completely (data not shown). After 30 s of exchange, helices A and C exhibit lower deuterium uptake than the rest of the molecule in the Ca-free state (Fig. 1a). Helices F, G and H are clearly protected in the Ca-saturated state relative to the Ca-free state.

The segments of TnC alone span a wide range of exchange rate constants (Table 1). The N-terminal helix (aa 1–8) exchanges with a rate constant of 3000 h^{-1} in the Ca-free state, decreasing 1.5-fold upon Ca^{2+} binding. However, the rate constant for the loop between helices N and A (aa 9–14) increases ~6-fold upon Ca^{2+} addition. Helix A (aa 15–27) exhibits two amide hydrogen exchange rate constants in the Ca-free state but only one in the Ca-saturated state. The loop between helices A and B as well as helix B (aa 28–41) exhibits two different rate constants that are not significantly affected by Ca^{2+} addition. The loop between helices B and C (aa 48–53) shows two HDX rates in the Ca-free state but only one (fast) rate in the Ca-saturated state. Helix C (aa 54–63) exhibits two rates, not affected by Ca^{2+}. The loop between helices C and D (aa 64–74) shows two different rate constants in both states. However, Ca^{2+} addition induces a 6- to 8-fold increase in both rate constants and a shift in the amide hydrogen populations toward faster exchange (55:45 vs. 80:20).

The DE linker between the N- and the C-lobes of TnC (aa 81–100) exchanges rapidly in both states and is unaffected by Ca^{2+}. The loop between helix E and F (aa 105–113) showed a decrease of ~3.5 orders of magnitude in the rate constant for 55% of the amide hydrogens on Ca^{2+} binding. Helix F (114–123) showed a similar Ca^{2+}-induced decrease in rate constants for 75% of its amide hydrogens. The loops between helices F and G (aa 124–129), helices G and H (aa 141–149) as well as helix G (aa 130–140) exchange rapidly and are insensitive to Ca^{2+} with the exception of 20% of amide hydrogens for aa 133–149 that exhibit a 4-order-of-magnitude

Table 2
Hydrogen/deuterium exchange rate constants for TnC and TnI in the binary complex fragments in the Ca-saturated and Ca-free states. Notation as for Table 1.

TnC	Rate for Ca-free (h^{-1})	TnC	Rate for Ca-saturated (h^{-1})
1–8	2100	1–8	2400
9–12	470		
24–27	2.1	24–27	4.6 (20%) and 0.14 (80%)
28–41	280 (70%) and 3.0 (30%)	28–41	250 (65%) and 3.8 (35%)
96–100	2600	96–100	260
101–104	0.21		
119–123	2100 (20%) and 1.2 (80%)	119–123	3.1
132–148	160 (10%) and 0.025 (90%)		
150–153	130 (5%) and 0.071 (95%)	150–153	210 (25%) and 0.79 (75%)
154–161	6.8 (30%) and 0.050 (70%)	154–161	96 (45%) and 1.2 (55%)
TnI	**Rate for Ca-free (h^{-1})**	**TnI**	**Rate for Ca-saturated (h^{-1})**
1–25	370	1–25	350 (95%) and 2.6 (5%)
30–52	520 (65%) and 1.7 (35%)	30–52	270 (75%) and 1.4 (25%)
53–60	2.2		
70–90	2300	76–96	420
91–96	480		
109–133	1500	109–133	420
153–158	450	147–158	310
165–169	2300		
170–179	180		
189–193	300	190–195	370 (95%) and 1.5 (5%)
197–210	1400	197–210	570 (90%) and 3.7 (10%)

Table 3
Hydrogen/deuterium exchange rate constants for each of the Tn subunits in the ternary complex in the Ca-saturated and Ca-free states. Notation as for Table 1.

TnC	Rate for Ca-free (h^{-1})	TnC	Rate for Ca-saturated (h^{-1})
1–8	2000	1–8	2000
9–17	1000 (75%) and 16 (25%)	9–17	2600 (75%) and 15 (25%)
18–23	560 (30%) and 1.4 (70%)		
24–27	16 (10%) and 0.64 (90%)	24–27	0.35
28–41	1100 (85%) and 2.7 (15%)	28–41	240 (90%) and 2.7 (10%)
58–62	1400 (95%) and 1.8 (5%)		
105–113	280 (70%) and 6.2 (30%)	105––113	2100 (40%) and 1.6 (60%)
114–118	210 (35%) and 7.8 (65%)	114–118	83 (25%) and 0.34 (75%)
124–132	320		
135–149	250 (85%) and 1.4 (15%)	132–149	690 (55%) and 1.4 (45%)
150–153	100 (55%) and 4.9 (45%)	150–153	110 (15%) and 0.23 (85%)
154–161	50 (70%) and 2.2 (30%)	154–161	390 (50%) and 6.2 (50%)
TnI	Rate for Ca-free (h^{-1})	TnI	Rate for Ca-saturated (h^{-1})
1–29	530	1–29	710
30–52	500 (80%) and 1.6 (20%)	30–52	660 (85%) and 0.44 (15%)
53–60	0.012	53–60	0.013
61–76	240 (50%) and 2.3 (50%)	61–76	164 (45%) and 2.7 (55%)
77–92	200 (90%) and 2.3 (10%)	77–92	330 (80%) and 3.7 (20%)
93–96	1600 (45%) and 0.52 (55%)	93–96	1000 (35%) and 0.48 (65%)
109–115	3800 (30%) and 0.066 (70%)	109–115	940 (45%) and 0.26 (55%)
116–126	17 (20%) and 0.72 (80%)	116–126	200 (25%) and 0.64 (75%)
127–133	1.2 (30%) and 0.032 (70%)	127–133	1.5 (40%) and 0.11 (60%)
147–152	450	147–152	2500
156–165	580	156–165	230
166–210	380	166–210	2100
TnT	Rate for Ca-free (h^{-1})	TnT	Rate for Ca-saturated (h^{-1})
1–31	390	1–22	480
43–70	400	43–70	660
71–87	420	71–87	1700
100–127	280	100–127	240
128–156	2800	128–177	1500
158–181	500		
186–219	440	178–212	380
220–227	210 (95%) and 3.5 (5%)	220–232	170 (70%) and 1.6 (30%)
228–236	10 (20%) and 0.49 (80%)		
237–242	39	237–242	180 (35%) and 0.040 (65%)
254–262	2.0 (45%) and 0.049 (55%)	254–262	12 (30%) and 0.82 (70%)
263–288	400	263–288	1600

decrease in the rate constant. A 4-order-of-magnitude decrease in the exchange rate constant was also observed for helix H (aa 150–155) upon Ca^{2+} addition. The rate constants for the C-terminal segment (aa 156–161) decreased by half for 70% of its amide hydrogens and by 2 orders of magnitude for the other 30%.

3.2. The binary TnC:TnI complex

The formation of the binary TnC:TnI complex limits protease accessibility, so that proteolytic digestion produced large fragments (>40 aa). The sequence coverage of TnC based on fragments with an average length of 9 aa (not including the large fragments) was ~40% for the Ca-free and the Ca-saturated states. TnI sequence coverage was 70% in the Ca-free and 60% in the Ca-saturated states (Fig. 1b). For TnC, the white-colored C-terminal segment of helix E, the loop between helices E and F, and the N-terminal segment of helix F incorporate deuterium slowly in both states. The same domain has a higher deuterium uptake for TnC alone. The N-lobe of TnC exhibits Ca-sensitive protection (Fig. 1b). For TnI, the deuterium uptake for the N-terminal segment of helix 1 (aa 40–48) is higher than that from an adjacent segment (aa 49–58) in both Ca states. However, the former exhibits Ca-induced protection whereas the latter becomes slightly exposed upon Ca^{2+} addition. Helix 2 of TnI exchanges rapidly and is not affected by Ca^{2+}. ~75% of the amide hydrogens of the TnI N-terminal extension (aa 1–25) exchange for deuterium after 30 s of exposure to D_2O. Ca^{2+} addition slightly reduces the deuterium uptake (Fig. 2 left).

For the binary TnC:TnI complex, the exchange rate constants of the N-terminal helix of TnC (aa 1–8) are similar for the Ca-free and the Ca-saturated states (Table 2). For the Ca-free state, the loop between helices N and A (aa 9–12) shows a 4-fold decrease in the rate constant relative to the N helix. Most amide hydrogens in the C-terminal segment of helix A (aa 24–27) exhibit Ca-induced protection, evidenced by a 15-fold decrease in the exchange rate constants. In contrast to TnC alone, the loop between helices A and B as well as helix B (aa 28–41) in the binary complex reveal no Ca-dependence. The N-terminal segment of helix E (aa 96–100) shows a 10-fold decrease in the exchange rate constant upon Ca^{2+} binding. The C-terminal fragment of the same helix (aa 101–104) was observed only in the Ca-free state and shows a rate constant 4 orders of magnitude lower than that for the N-terminal segment (aa 96–100). For the C-terminal segment of helix F (aa 119–123), 20% of the amide hydrogens exhibit a ~3-order-of-magnitude Ca-induced decrease in rate constant. The remaining 80% exchange at practically the same rate for both Ca states. Helix G and the loop between helices G and H (aa 132–148) were observed only for the Ca-saturated state. Most of the amide hydrogens in segments exchange very slowly ($0.025\,h^{-1}$). Upon Ca^{2+} addition, an order-of-magnitude increase in the rate constant was observed for most amide hydrogens in helix H (aa 150–153). The C-terminus of TnC (aa 154–161) undergoes relatively slow exchange and exhibits 10- to 20-fold Ca-induced increase in rate constant.

On the other hand, the N-terminal extension of TnI (aa 1–25) exchanges at $\sim 350\,h^{-1}$ for both Ca states. Two populations of

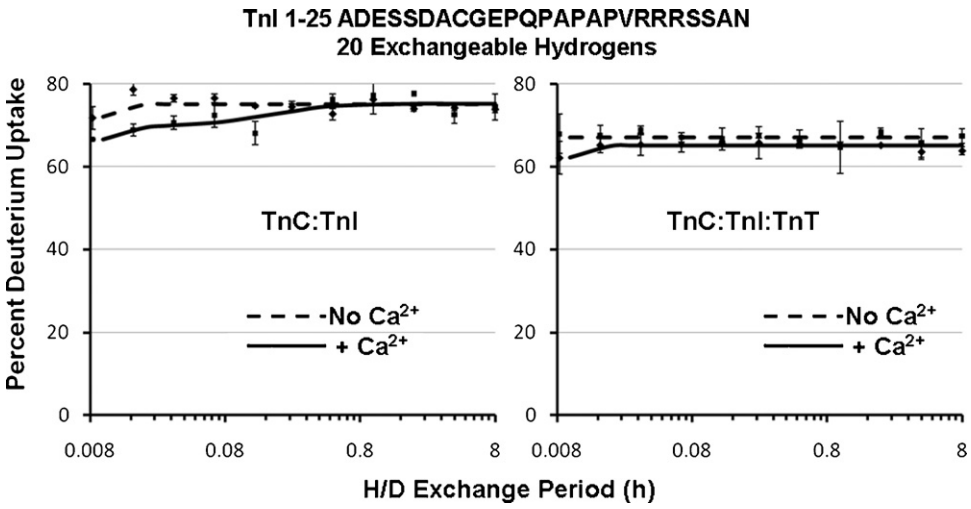

Fig. 2. Deuterium uptake vs. time for the N-terminal extension of TnI in the binary TnC:TnI complex (left) and the ternary TnC:TnI:TnT complex (right). The lines correspond to two-exponential fits for the Ca-free state (— — —) and the Ca-saturated state (—). The exchange is very fast for both states and is not significantly affected by Ca^{2+} addition.

amide hydrogens exchange at different rates in the N-terminal fragment of TnI helix 1 (aa 30–52), with a 2-fold Ca-sensitive decrease in the larger rate constant. The loop between helices 1 and 2 exchanges five times slower for the Ca-saturated state than the Ca-free state. The rate constant for the C-terminal segment of helix 2 (aa 109–133) decreases 3.5-fold upon Ca^{2+} addition. Part of the switch peptide (aa 153–158) shows no Ca-induced change in the exchange rate constant. The C-domain of TnI (aa 165–169, 170–179, 189–193 and 197–210) exchanges relatively rapidly for the Ca-free state (200–2000 h^{-1}). Only the aa 197–210 segment exhibits a 3-fold decrease in rate constant upon Ca^{2+} addition.

3.3. The ternary TnC:TnI:TnT complex

Proteolytic digestion of the ternary complex produced very few fragments. Therefore, urea was added after the exchange reaction and during the quench/digestion. The sequence coverage was 60% for TnC and 88% for both TnI and TnT based on fragments with average length of ~10 aa. Fig. 1c shows deuterium uptake in the ternary complex after 30 s of exposure to D_2O. Helices A, F and H exchange slower than the rest of the subunit. Parts of helices F, G and H and the loops that connect them reveal Ca-induced protection of the C-lobe of TnC (Supplemental Fig. 1). For TnI, the N-terminal extension was unaffected by Ca^{2+} addition (Fig. 2 right). The same pattern of deuterium uptake was observed for the N-terminal segment of helix 1 in the binary and the ternary complexes (Fig. 1b and c). Helix 2 of TnI exchanged slowly, as indicated by the white color for both Ca states. The amide hydrogens of the switch peptide (aa 147–152) (Supplemental Fig. 2) as well as the C-terminal part of the TnI mobile domain (aa 180–210) exchange faster in the Ca-saturated than in the Ca-free states (Fig. 1c). Helix 1 of TnT2 displays Ca-sensitive protection, whereas helix 2 (which constitutes the coiled-coil) exchanges slowly in both states and is not affected by Ca^{2+}. However, the C-terminal segment of that helix (aa 263–288) exchanges rapidly (darker green) and exhibits opening upon Ca^{2+} binding.

Table 3 lists the exchange rate constants for the subunits of the ternary TnC:TnI:TnT complex. For TnC, helix N (aa 1–8) is not affected by Ca^{2+} addition and the exchange is relatively fast. The end segment of helix N, the loop between helix N and helix A, and the beginning segment of helix A (aa 9–17) exhibit two different exchange rate constants, one of which doubles upon Ca^{2+} binding. The central segment of helix A (aa 18–23) was observed only for the Ca-free state and the amide hydrogen populations shift toward slower rates. Amino acids 24–27 undergo the slowest exchange for TnC, and Ca^{2+} lowers the rate constant 2-fold. The loop between helices A and B as well as helix B (aa 28–41) exhibit a similar decrease (~4.5-fold) for most of the amide hydrogens. Helix C (aa 58–62) was observed only for the Ca-free state and exchanges at 1400 h^{-1}. The amide hydrogens of the loop between helices E and F (aa 105–113) undergo a Ca-induced, 7.5-fold increase in the largest rate constant and a 4-fold decrease in the lowest. Those changes are accompanied by a shift in the populations toward the lower rate constant. Ca^{2+} also induces a 2.5-fold decrease in the rate constant of one population and a 23-fold decrease in the other for aa 114–118 of helix F. Helix G and the loop between helices G and H (aa 135–149) reveal two populations in the Ca-free state: the first (85% of the amide hydrogens) exchanges at 250 h^{-1} and the other (15%) exchanges at 1.4 h^{-1}. Upon Ca addition, 30% of the hydrogens in the first population now exchange with the rate constant of the second population and the remaining 55% exhibit a 2.5-fold increase in rate constant. A similar pattern was observed for aa 150–153 of helix H with the exception that the first population has the same rate constant in both Ca states but the second exhibits a 21-fold decrease in the rate constant upon Ca^{2+} addition. A Ca-induced increase in the rate constant was observed for most of the amide hydrogens from the C-terminus of TnC (aa 154–161).

The TnI N-terminal extension (aa 1–29) exchanges at ~500 h^{-1} and is not sensitive to Ca^{2+}. The N-terminal segment of helix 1 (aa 30–52) exhibits a 4-fold decrease in the smallest rate constant. The middle segment of helix 1 (aa 53–60) shows the slowest exchange in the complex and no Ca-dependence. The C-terminal segment of helix 1, the loop between helices 1 and 2, as well as the N-terminal segment of helix 2 (aa 61–76, 77–92 and 93–96) exhibit similar Ca^{2+} insensitivity. In helix 2, aa 109–115 and 127–133 were characterized by a relatively slow exchange and a 3- to 4-fold Ca-induced increase in the rate constants of most of the amide hydrogens. However, most of the amide hydrogens in residues 116–126 are insensitive to Ca^{2+}. We also noted a 5-fold increase in the rate constant of the switch peptide (aa 147–152) upon Ca^{2+} addition. Amino acids 156–165 exhibit slightly decreased rate constant but the C-terminal domain (aa 166–210) experienced a 4.5-fold increase in rate constant upon Ca^{2+} addition.

Finally, TnT1 (aa 1–181), which was not included in the crystal structure reveals a uniform and fast exchange (~400 h^{-1}) with

no Ca-induced changes except for the following peptides. Amino acids 71–87 and 128–156 exhibit four times faster and twice slower exchange for the Ca-saturated relative to the Ca-free state. The N-terminal half of the TnT2 helix 1 (aa 186–219) exchanges at the same rate as TnT1 and is not affected by Ca^{2+}. The loop between TnT2 helices 1 and 2 (aa 220–227) exhibits slightly decreased rate constants but more important, a shift of 25% of the amide hydrogens toward slower exchange. Upon Ca^{2+} binding, the peptides of helix 2 (aa 228–262) exhibit 5- to 15-fold increase in the rate constant, except for aa 237–242 for which 65% of the amide hydrogens show ~3 order-of-magnitude Ca-induced decrease in the rate constant. The C-terminus of TnT2 (aa 263–288) exchanges rapidly and exhibits a 4-fold Ca-induced increase in the rate constant.

4. Discussion

The spatial resolution of the HDX technique is limited by the lengths of the fragments produced by proteolytic digestion. Short fragment segments (~10 aa) provide localized information. Thus, although our reported sequence coverage would be considerably higher if we included the larger peptide fragments (especially for the binary complex), their poor spatial resolution would not significantly improve the analysis. The deuterium uptake data were mapped on the Ca-saturated crystal structure of Takeda et al. [5] for visualization purposes only and because that structure provides the closest model available for the binary and ternary complexes. Given the short timescale over which the dynamic aspects of the Tn complex occur (the rates of Ca^{2+} binding, conformational changes, and muscle activation), the deuterium uptake after 30 s of exchange is the most physiologically relevant and is represented in Fig. 1.

The exchange rate constants were computed by fitting the deuterium uptake time profiles to either one or two exponentials. They spanned a 5-order-of-magnitude range (0.01–1000 h^{-1}), indicating that the Tn complex possesses both highly flexible and very rigid domains. Most of the transitions occur before 30 s. Therefore any rate constant greater than 120 h^{-1} ($(1/30) \times 3600$) exhibits higher uncertainty and does not guarantee that the exchange happened in a single abrupt transition as assumed by the fitting algorithm. The highest exchange rates were observed for the DE linker of TnC alone, the N-terminal extension, and the mobile domain of TnI in the binary and ternary complexes. The slowest exchange was observed for the IT coiled-coil.

Variations in the rate constants are due to either secondary or tertiary structural changes in the subunits upon formation of the complex or allosteric effects induced by Ca binding to TnC. In other words, a decrease in the deuterium uptake could imply either a protection due to tertiary or quaternary interactions or *de novo* hydrogen bonding in the secondary structures.

4.1. TnC

TnC exhibits the most significant changes in rate constants upon complexation and Ca^{2+} addition. For TnC alone, Ca^{2+} binding to site II opens up the N-lobe and protects the C-lobe, as denoted by the red and blue colors in Fig. 1a and the lower deuterium uptake time profiles in Supplemental Fig. 1. The N-lobe conformational changes were previously reported as opening of a hydrophobic cleft by either NMR [18,21] or X-ray crystallography [19,20]. The opening of the N-lobe translates into a 3- to 8-fold Ca-induced increase in the rate constants of most amide hydrogens in that domain (Table 1). However, the increase in solvent access for the N-lobe is replaced by protection as soon as TnI is added to TnC (Fig. 1b and c, and Supplemental Fig. 2), due to interaction with TnI switch peptide [5,9]. The Ca-induced protection in the C-lobe is a new implication also reported by the recent HDX FT-ICR work of Kowlessur and Tobacman [29].

Ca^{2+} also caused orders-of-magnitude decrease in the rate constants for the majority of the amide hydrogens in the C-lobe of TnC alone (see Section 3 and Table 1). The decrease was not as pronounced for the ternary complex, presumably because of the interaction with TnI and TnT [5,6,22,23], suggesting that the allosteric changes observed in the C-lobe of TnC are transmitted to produce other conformational changes in TnI and TnT. In both the Ca-free and the Ca-saturated states, the rate constants for the C-lobe amide hydrogens in the binary and ternary complexes were one order of magnitude smaller than those for TnC alone (Tables 1–3), confirming the interaction between the C-lobe of TnC and the N-terminal segment of TnI helix 1 [22,23]. The DE linker, observed only for TnC alone, exchanges very rapidly and is not affected by Ca^{2+}, confirming the disordered character of that domain observed by Takeda et al. [5] However, in the binary complex, the N-terminal half of helix E exhibits an order of magnitude decrease in the exchange rate constant upon Ca^{2+} addition (Table 2), possibly due to an interaction between the inhibitory peptide of TnI and the DE linker of TnC in the Ca-saturated state reported originally in skeletal Tn [6] and recently in cardiac Tn [29].

4.2. TnI

The N-terminal extension of TnI, found only in the cardiac isoform, exchanges rapidly in both the binary and ternary complexes (Tables 2 and 3). Although a small change in deuterium uptake could be observed upon addition of Ca^{2+} to the binary complex (Fig. 2), the decrease is minimal and cannot be considered significant, consistent with the small population (5%) of amide hydrogens that exhibit a change in the rate constant upon Ca^{2+} binding (Table 2). Overall, complexation and Ca^{2+} addition did not affect the exchange and therefore the solvent accessibility for the N-terminal extension.

The amino-terminal segment of TnI helix 1 shows two different exchange rates in each of the binary and ternary complexes (Tables 2 and 3). The slow component is attributed to interaction with the C-lobe of TnC as discussed above [22]. In the binary complex, the fast rate decreases by a factor of 2 upon Ca-addition (Table 2). However, that decrease was not observed for the ternary complex for the major component, presumably because of the additional stability acquired from the interaction of TnI helix 2 with TnT helix 2 (IT coiled-coil) [5]. The slow exchange rate for the middle segment of TnI helix 1 most likely results from the strong hydrogen bonding in the helix. The rate constants for the C-terminal part of helix 1, the loop between helix 1 and helix 2, and the N-terminal part of helix 2 that exhibit a 5-fold Ca-induced decrease in the binary complex were not affected by Ca^{2+} in the ternary complex (Tables 2 and 3). Evidently, TnT binding decreases the Ca-induced long-range effects by rendering additional stiffness and stability to the ternary complex (also reported by Kowlessur and Tobacman [29]).

In the binary complex, the C-terminal segment of TnI helix 2 exchanges at a single fast rate that decreases 3.5-fold upon Ca^{2+} binding. For the ternary complex, the amide hydrogens of the same fragment comprise two populations that exchange at significantly lower rates than in the binary complex (Tables 2 and 3). Ca^{2+} slightly speeds the exchange rates for both populations and increases the slow rate constant 3- to 4-fold. In the binary complex, helix 2 of TnI readily exchanges after 30 s of exposure to D_2O (Fig. 1b). However, in the ternary complex the same helix incorporates less than 10% deuterium even after 8 h of exchange (data not shown): hence the slow exchange rates. Briefly, the strong interaction between TnT helix 2 and TnI helix 2 (the IT coiled-coil) grants additional stability

to the ternary complex but does not prevent long-range Ca-induced allosteric changes.

The N-terminal residues (aa 147–152) of the switch peptide exhibit a 5-fold *increase* in exchange rate upon Ca^{2+} binding to the ternary complex (Table 3). That result was unexpected because the switch peptide is proximal to the TnC N-lobe in the Ca-saturated state, [5,9] for which protection was observed and was discussed earlier (Supplemental Fig. 2). However, the C-terminal residues (aa 156–165) exhibit a 2.5-fold *decrease* in exchange rate constant upon Ca-addition (Table 3). Nevertheless, the increase in the rate constant could be explained by binding of the switch peptide to the hydrophobic pocket of TnC, inducing local unfolding in the N-terminal and resulting in faster exchange. That assumption also explains the Ca-induced 5.5-fold increase in the exchange rate constant for the residues of the C-terminal domain of TnI (also known as the mobile domain).

4.3. TnT

TnT1 was not included in previous structural studies. It does not interact with the core domain and serves to dock the Tn complex to Tm [16]. Here, we find that TnT1 exchanges rapidly in both Ca states and exhibits a 4-fold increase in exchange rate constant for aa 71–87 and a 2-fold decrease for aa 128–156 upon Ca^{2+} addition (Table 3). The fast exchange might be expected, given that we did not include Tm and actin. However, the observed Ca-induced changes might be needed to reposition Tm on actin, thereby inducing muscle contraction [40].

TnT2 has been included in all Tn ternary complex crystal structures solved to date [5,6]. Helix 1 behaves like TnT1 and is not affected by Ca^{2+}: reasonable, given that TnT2 helix 1 is a continuous extension of TnT1. However, the loop between helices 1 and 2 exhibits slower exchange in the Ca-saturated state relative to the Ca-free state (Table 3). Other Ca-induced changes were also observed in helix 2, which exchanges slowly in both states due to interaction with TnI helix 2 (IT coiled-coil). The C-terminal segment of helix 2 is proximal to the TnC C-lobe in the Ca-saturated crystal structure, [5] and exhibits a Ca-induced increase in exchange rate constant, implying that protection is greater in the Ca-free state due to stronger interaction with the C-lobe of TnC. That interpretation is further confirmed by the decrease in protection for the C-lobe in the ternary complex relative to TnC alone.

5. Conclusion

We have illuminated the structural role of each subunit of the Tn complex as well as structural changes induced by Ca^{2+} binding, by use of HDX monitored by FT-ICR mass spectrometry. The decrease in exchange rate constants for the ternary complex relative to TnC alone or the binary complex indicates that the formation of the IT coiled-coil stabilizes Tn. In TnC alone, Ca^{2+} binding to site II of the N-lobe leads to allosteric opening of the hydrophobic cleft and protection for the C-lobe. The degree of protection for the C-lobe decreases in the binary and ternary complexes due to interaction with TnI and TnT. Long-range allosteric effects are also observed in the IT coiled-coil and in some parts of TnT1. A broader understanding of the Ca-regulated contraction requires the presence of Tm and actin. The present data are consistent with prior crystallographic and NMR results as well as recent HDX experiments, and reveal additional structural details about non-resolved and truncated domains such as the N-terminal extension of TnI. That extension is specific to the cardiac isoform, is highly flexible, and is insensitive to Ca^{2+}. Further work will focus on the structure and dynamics implications of phosphorylation of Ser 22 and Ser 23 in the extension.

Acknowledgments

The authors thank Erik Stapleton for help in the protein expression and purification. This work was supported by NIH (GM 78359), NSF (DMR-0654118), The American Heart Association (TIA-2280172 and 09-PRE-2130013) and the State of Florida.

Appendix A. Supplementary data

Supplementary data associated with this article can be found, in the online version, at doi:10.1016/j.ijms.2010.08.023.

References

[1] A.M. Gordon, E. Homsher, M. Regnier, Physiological Reviews 80 (2000) 853–924.
[2] M.S. Parmacek, R.J. Solaro, Progress in Cardiovascular Diseases 47 (2004) 159–176.
[3] A.V. Gomes, J.D. Potter, D. Szczesna-Cordary, IUBMB Life 54 (2002) 323–333.
[4] A.M. Gordon, M. Regnier, E. Homsher, News in Physiological Sciences 16 (2001) 49–55.
[5] S. Takeda, A. Yamashita, K. Maeda, Y. Maeda, Nature 424 (2003) 35–41.
[6] M.V. Vinogradova, D.B. Stone, G.G. Malanina, C. Karatzaferi, R. Cooke, R.A. Mendelson, R.J. Fletterick, Proceedings of the National Academy of Sciences of the United States of America 102 (2005) 5038–5043.
[7] S.K. Sia, M.X. Li, L. Spyracopoulos, S.M. Gagne, W. Liu, J.A. Putkey, B.D. Sykes, Journal of Biological Chemistry 272 (1997) 18216–18221.
[8] L. Spyracopoulos, M.X. Li, S.K. Sia, S.M. Gagne, M. Chandra, R.J. Solaro, B.D. Sykes, Biochemistry 36 (1997) 12138–12146.
[9] M.X. Li, L. Spyracopoulos, B.D. Sykes, Biochemistry 38 (1999) 8289–8298.
[10] R. Zhang, J.J. Zhao, J.D. Potter, Journal of Biological Chemistry 270 (1995) 30773–30780.
[11] S.U. Reiffert, K. Jaquet, L.M.G. Heilmeyer, M.D. Ritchie, M.A. Geeves, FEBS Letters 384 (1996) 43–47.
[12] B.A. Levine, A.J.G. Moir, S.V. Perry, European Journal of Biochemistry 172 (1988) 389–397.
[13] R.T. McKay, B.P. Tripet, R.S. Hodges, B.D. Sykes, Journal of Biological Chemistry 272 (1997) 28494–28500.
[14] Y. Luo, J. Leszyk, Y.D. Qian, J. Gergely, T. Tao, Biochemistry 38 (1999) 6678–6688.
[15] T.M.A. Blumenschein, D.B. Stone, R.J. Fletterick, R.A. Mendelson, B.D. Sykes, Biophysical Journal 90 (2006) 2436–2444.
[16] S.P. White, C. Cohen, G.N. Phillips, Nature 325 (1987) 826–828.
[17] I. Ohtsuki, K. Yamamoto, K. Hashimoto, Journal of Biochemistry 90 (1981) 259–261.
[18] S.M. Gagne, S. Tsuda, M.X. Li, L.B. Smillie, B.D. Sykes, Nature Structural Biology 2 (1995) 784–789.
[19] M. Sundaralingam, R. Bergstrom, G. Strasburg, S.T. Rao, P. Roychowdhury, M. Greaser, B.C. Wang, Science 227 (1985) 945–948.
[20] O. Herzberg, M.N.G. James, Nature 313 (1985) 653–659.
[21] C.M. Slupsky, B.D. Sykes, Biochemistry 34 (1995) 15953–15964.
[22] G.M.C. Gasmi-Seabrook, J.W. Howarth, N. Finley, E. Abusamhadneh, V. Gaponenko, R.M.M. Brito, R.J. Solaro, P.R. Rosevear, Biochemistry 38 (1999) 8313–8322.
[23] D.G. Vassylyev, S. Takeda, S. Wakatsuki, K. Maeda, Y. Maeda, Biophysical Journal 74 (1998) A53.
[24] T.E. Wales, J.R. Engen, Mass Spectrometry Reviews 25 (2006) 158–170.
[25] D.L. Smith, Y.Z. Deng, Z.Q. Zhang, Journal of Mass Spectrometry 32 (1997) 135–146.
[26] S.W. Englander, Journal of the American Society for Mass Spectrometry 17 (2006) 1481–1489.
[27] A.G. Marshall, C.L. Hendrickson, International Journal of Mass Spectrometry 215 (2002) 59–75.
[28] A.G. Marshall, C.L. Hendrickson, G.S. Jackson, Mass Spectrometry Reviews 17 (1998) 1–35.
[29] D. Kowlessur, L.S. Tobacman, Journal of Biological Chemistry 285 (2010) 2686–2694.
[30] W.J. Dong, J. Xing, M. Villain, M. Hellinger, J.M. Robinson, R. Chandra, R.J. Solaro, P.K. Umeda, H.C. Cheung, Journal of Biological Chemistry 274 (1999) 31382–31390.
[31] W.J. Dong, M. Chandra, J. Xing, M.D. She, R.J. Solaro, H.C. Cheung, Biochemistry 36 (1997) 6754–6761.
[32] M.D. She, J. Xing, W.J. Dong, P.K. Umeda, H.C. Cheung, Journal of Molecular Biology 281 (1998) 445–452.
[33] G.M. Bou-Assaf, J.E. Chamoun, M.R. Emmett, P.G. Fajer, A.G. Marshall, Analytical Chemistry 82 (2010) 3293–3299.
[34] J.D. Potter, J. Gergley, The Journal of Biological Chemistry 250 (1975) 4628–4633.

[35] H.M. Zhang, S.M. McLoughlin, S.D. Frausto, H.L. Tang, M.R. Emmettt, A.G. Marshall, Analytical Chemistry 82 (2010) 1450–1454.
[36] H.M. Zhang, G.M. Bou-Assaf, M.R. Emmett, A.G. Marshall, Journal of the American Society for Mass Spectrometry 20 (2009) 520–524.
[37] M.R. Emmett, F.M. White, C.L. Hendrickson, S.D.H. Shi, A.G. Marshall, Journal of the American Society for Mass Spectrometry 9 (1998) 333–340.
[38] S. Kazazic, C.L. Nilsson, M.R. Emmett, A.G. Marshall, Key West, Florida, 2005.
[39] S. Kazazic, H.-M. Zhang, T.M. Schaub, M.R. Emmett, C.L. Hendrickson, G.T. Blakney, A.G. Marshall, Journal of the American Society for Mass Spectrometry 21 (2010) 550–558.
[40] D.F.A. Mckillop, M.A. Geeves, Biophysical Journal 65 (1993) 693–701.